

Underwater Image Enhancement Using Adaptive Retinal Mechanisms

Shao-Bing Gao[✉], Member, IEEE, Ming Zhang[✉], Qian Zhao, Xian-Shi Zhang[✉], and Yong-Jie Li[✉], Senior Member, IEEE

Abstract—We propose an underwater image enhancement model inspired by the morphology and function of the teleost fish retina. We aim to solve the problems of underwater image degradation raised by the blurring and nonuniform color biasing. In particular, the feedback from color-sensitive horizontal cells to cones and a red channel compensation are used to correct the nonuniform color bias. The center-surround opponent mechanism of the bipolar cells and the feedback from amacrine cells to interplexiform cells then to horizontal cells serve to enhance the edges and contrasts of the output image. The ganglion cells with color-opponent mechanism are used for color enhancement and color correction. Finally, we adopt a luminance-based fusion strategy to reconstruct the enhanced image from the outputs of ON and OFF pathways of fish retina. Our model utilizes the global statistics (i.e., image contrast) to automatically guide the design of each low-level filter, which realizes the self-adaption of the main parameters. Extensive qualitative and quantitative evaluations on various underwater scenes validate the competitive performance of our technique. Our model also significantly improves the accuracy of transmission map estimation and local feature point matching using the underwater image. Our method is a single image approach that does not require the specialized prior about the underwater condition or scene structure.

Index Terms—Underwater image processing, biologically inspired vision, color correction.

I. INTRODUCTION

UNDERWATER images often suffer from noise, color distortion and low contrast, because light is attenuated when it propagates through water. These problems increase the difficulty of various tasks such as automatic fish and plankton detection and recognition. Therefore, many methods have been proposed to recover or enhance the degraded underwater images [1].

Manuscript received January 21, 2019; revised April 21, 2019; accepted May 24, 2019. Date of publication June 10, 2019; date of current version August 28, 2019. This work was supported in part by the National Natural Science Foundation of China under Grant 61806134, in part by the Fundamental Research Funds for the Central Universities under Grant YJ201751, and in part by the Sichuan Province Science and Technology Support Project under Grant 2017JY0249, Grant 2017SZ0004, and Grant 2017SZDZX0019. The associate editor coordinating the review of this manuscript and approving it for publication was Prof. Dong Xu. (*Corresponding author: Yong-Jie Li*.)

S.-B. Gao was with the School of Life Science and Technology, University of Electronic Science and Technology of China (UESTC), Chengdu 610054, China. He is now with the College of Computer Science, Sichuan University, Chengdu 610065, China (e-mail: gaoshaobing@scu.edu.cn).

M. Zhang, Q. Zhao, X.-S. Zhang, and Y.-J. Li are with the Center for Information in BioMedicine, School of Life Science and Technology, University of Electronic Science and Technology of China, Chengdu 610054, China (e-mail: zm_uestc@163.com; zhangxianshi@uestc.edu.cn; liyj@uestc.edu.cn).

Digital Object Identifier 10.1109/TIP.2019.2919947

The noise reduction methods for underwater images could be roughly classified as wavelet-based and filter-based [2], [3]. Some algorithms consider the forward and backward scattering components for removing the noise and improving the global contrast [4]. The operation of color correction aims to reduce the strong color cast that typically exists in underwater images [5], [6]. Many strategies aim for a visually pleasing result, but without the capability of realizing color constancy (CC) that is required for robust color-vision based applications [7]–[11].

Recently, many CC methods have been built on the purpose of retrieving the true colors of scenes and the results of underwater images after CC could be quantitatively evaluated [10], [12]. However, applying the conventional CC methods specifically designed for terrestrial environments on underwater images will lead to the undesired artifacts since the red component of an underwater image is generally much weaker than its blue and green components. Hence, many CC methods have been modified to adapt the underwater environment.

Henke *et al.* [13] make an assumption that the average reflectance is achromatic at the same level of attenuation. Ancuti *et al.* [14] develop a compensation version of shades-of-grey to white-balance the underwater images. They further exploit an optional channel compensation mechanism [9] to suppress the possible red artifacts induced by the conventional gray-world based methods. All of these methods are based on the uniform color cast assumption. In practice, the color cast depends on both the water type and the 3D structures of the scenes, making the uniform CC of underwater images invalid. Recently, Berman *et al.* [10], [15] utilize the prior of the spectral profiles of different water bodies for nonuniform CC and quantitatively evaluate their method on a new underwater dataset with varying color casts taken in different locations. Moreover, several deep learning-based approaches exploiting the image style translation mechanisms are recently developed to generate the enhanced underwater images [16]–[18].

Many enhancement algorithms (e.g., [12], [19]–[21]) for underwater images are built on the dark channel prior (DCP) based dehazing mechanisms [22], [23]:

$$I_\lambda(x, y) = J_\lambda(x, y)t(x, y) + A_\lambda(1 - t(x, y)) \quad (1)$$

where $I_\lambda(x, y)$ denotes the captured underwater image, $J(x, y)$ denotes the true image without degradation, $t(x, y)$

is the transmission and A is the homogeneous background light. The purpose of dehazing is to retrieve $J_\lambda(x, y)$ from $I_\lambda(x, y)$ without knowing the values of A_λ and $t(x, y)$. Early underwater imaging techniques employ the specialized hardwares [24] and multiple images polarized over diverse angles [25]. Recently, inspired by outdoor dehazing [26], several DCP based solutions for underwater images have been introduced [12], [19], [21], [27], [28]. For example, Chiang and Chen [12] segment the foreground of the scene based on a depth estimate resulting from the DCP [26]. Galdran *et al.* [21] introduce the red channel transmission to recover the colors associated with the short wavelengths in underwater. These methods rely on the estimation of $t(x, y)$ and A_λ , which require specialized priors. Our proposed model essentially does not rely on the DCP-based dehazing mechanisms, which is advantageous since DCP may not always hold true [29], [30]. Besides, without using DCP, Ancuti *et al.* [9] propose to fuse the advantages of color balancing and enhancement. We follow this spirit to design an underwater image enhancement model using the adaptive retinal mechanisms [31]–[33].

Specifically, we propose a teleost fish retina inspired image enhancement model to solve the blurring and nonuniform color biasing problems of underwater images. The main contributions are as follows. (i) We imitate the retinal feedback mechanisms from color-sensitive horizontal cells to cones to introduce a nonuniform CC processing, which can well handle the nonuniform color bias in underwater images compared to previous state-of-the-art methods (SOTAs) that are usually built on the assumption of uniform color bias (e.g., gray world assumption). The experiments show that the accuracy of DCP based transmission estimation benefits significantly from our proposed nonuniform CC method. (ii) A new sharpening operation modeling the color-opponent mechanisms of retinal ganglion cells is proposed for color enhancement and color correction, which is quite flexible to adjust the color appearance of underwater images. (iii) The center-surround opponent mechanisms of bipolar cells are used for flexibly filtering out the low-pass and band-pass frequencies of underwater images, which can effectively transfer the edge and contrast information to the output. (iv) The main model parameters of each low-level filter adapt according to the global contrast of the input image, mimicking the dynamic modulation of the surrounding region to the central part of the receptive field (RF) of a neuron.

The main hypothesis underlying our work is that the visual systems of ocean creatures have evolved to adapt to the natural statistics of the aquatic scenes [34]–[39]. Thus, modeling the perception and imaging mechanisms of the ocean creatures (their physical optics, photoreceptors and neurophysiological mechanisms) will certainly give us new insights to the information processing of underwater images [1], [24].

In section II, we briefly introduce the related retinal structure and function of teleost fish and their intrinsic relations to the underwater image degradation. The proposed model will be introduced in section III. We present qualitative and quantitative assessments of our model on the datasets captured

under various underwater environments in section IV and make conclusion in section V.

II. INTRODUCTION TO THE TELEOST FISH RETINA

In the ocean, it is quite challenging to obtain good visibility of objects at long distances due to the absorptive and scattering natures of seawater. The deeper the water is, the less chromatic and contrast variations the aquatic scenes contain. Previous studies indicate that many deep-sea species, particularly the crustaceans, cephalopods and fish, have evolved to own highly adapted deep-sea visual systems with the specific mechanisms of spatial resolution, contrast sensitivity and color discrimination [34]–[39].

The retinal structure of teleost fishes mainly consists of the photoreceptor, horizontal cell, bipolar cell, and ganglion cell. The diversity of fish's behaviors and the living environments results in various retinal architectures and functions [31]. Photoreceptors include the rod and cone cells. Fishes living in deep-sea only have rod cells in order to adapt to the weakly illuminated environments [32]. In contrast, fishes living in broad spectral environments possess color vision because their cone cells can differentiate spectral of different wavelengths. Cone cells with the structure of double-cone are generally sensitive to the longer wavelengths, while the cone cells with the structure of single cone are maximally sensitive to the shorter wavelengths [31]. In cyprinid fishes, the cone cells with double-cone structure make up nearly 50% of the cone cells [40], which may be the results of adaption to the bluish environments.

In fish retina, there are three types of cone-connected horizontal cells and one type of rod-connected cells [31], [41]–[43]. Horizontal cells possess the biggest RF in the retina, which mainly receive the input from photoreceptors and then produce the feedback signals to photoreceptors [44]. The feedback signals are considered important for discounting the widely existing nonuniform color bias and thus the fish visual system could adapt to the color variations of underwater environment (e.g., realizing the color constancy) [45]–[49]. The RF of bipolar cells presents a typical center-surround opponent structure. Based on the responsive pattern to stimulus, bipolar cells can be further classified into ON-center and OFF-center based types. The ON-center bipolar cells are excited by light stimulation at the RF center but are inhibited at the RF surround. The OFF-center bipolar cells exhibit the opposite properties. In the retina of some fishes, the bipolar cells also possess a color-opponent property. The spatial center-surround RFs with color-opponent mechanisms play roles in enhancing the contents of high-pass and band-pass frequencies of an underwater image and thus promoting the transfer of edges and color contrast to the output image [46], [48], [49], [51], [52].

As the last layer of retina, ganglion cells directly receive the input from the bipolar cells and thus have both the center-surround and the color-opponent RF structures [53], [54]. Abundant studies have shown that the ON-center type and OFF-center type ganglion cells are functionally asymmetric when encoding the visual signals [55]–[58]. For example, the ON-center ganglion cells can encode the information with

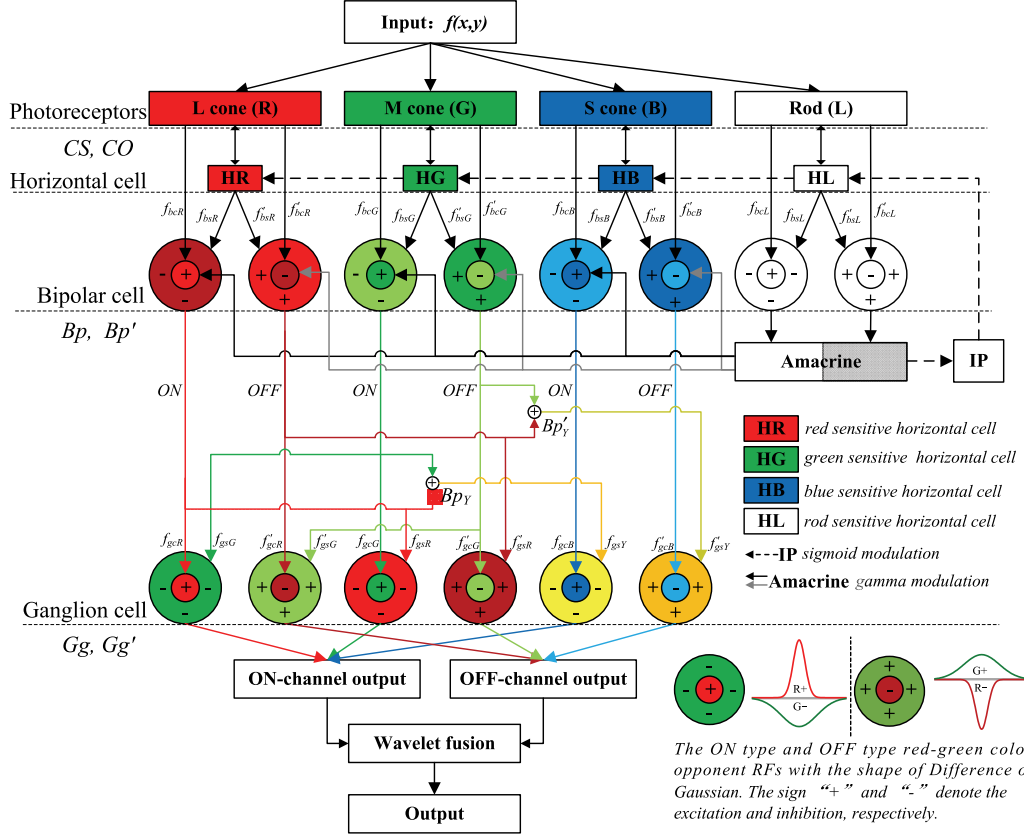


Fig. 1. The flowchart of the proposed model inspired by the fish retinal mechanisms. The HR, HG, HB denote the red (R), green (G) and blue (B) sensitive horizontal cells, respectively. The HL denotes the rod-connected horizontal cells. The components of R, G, B and brightness of the input color image are sent into the corresponding photoreceptors. The outputs of photoreceptors are modulated by the feedback of horizontal cell and then transmitted into the RF center of bipolar cell, while the outputs of horizontal cells after sigmoid modulation are transmitted into the RF surround of bipolar cell. The RF center of bipolar cell in the cone pathway also receives the input from the bipolar cell in the rod pathway after gamma modulation by the amacrine cell. The outputs of bipolar cells are transmitted into the color-opponent ganglion cells for further processing. The final output is obtained by integrating the outputs of ON- and OFF-ganglion cells (with a kind of the wavelet based fusion).

the relatively high luminance, while the OFF-center ganglion cells are more sensitive to the information with the relatively low luminance [58]. The retina thus selectively fuses the ON and OFF visual pathways to further enhance the details of the bright and dark parts of visual information, which makes the fish visual system highly sensitive to both the luminance and color defined boundaries. Moreover, the RF property of neurons highly depends on the contrast of the visual stimuli in the dynamic environment [33], [59].

III. THE FISH RETINA INSPIRED MODEL

As shown in Fig. 1, our model follows the basic visual signal processing mechanisms in the teleost fish retina.

A. Photoreceptors

As the first layer of retina, the photoreceptors can be classified into the rod and cone types, serving to transmit the received light signal into the neural response. Based on the sensitivity to the wavelength of the spectra, cone cells can be further separated into long (R), middle (G) and short (B) types [60]. We separate the underwater image $f(x,y)$ into R, G and B channels and treat them as the inputs

to cone cells. We simply define the luminance signal received by rod cells as

$$L(x, y) = (f_R(x, y) + f_G(x, y) + f_B(x, y))/3 \quad (2)$$

B. Horizontal Cells

Horizontal cells (HCs) have the biggest RF size in the retina, which makes it possible to integrate the signals from photoreceptors over relatively large regions. The feedback from HCs to photoreceptors is the first feedback path in the retina (e.g., the bidirectional arrow between the photoreceptors and HCs shown in Fig. 1), which is crucial to the realization of CC. In the existing CC models inspired by the retina mechanisms [61], the global mean of each of the R, G, B channels is used as the feedback of HCs to each cone type, which obviously neglects the nonuniform color variation of the underwater environment. Besides, the interplexiform cells also have the inhibitory regulation to horizontal cells, which is not considered by most of the retina based models. In our model, we use a local mean filter to simulate the RF of HCs, which first estimates the local light source colors from the input, and then returns the estimated local signal as the feedback to correct the signal encoded by the cone cells. Based on the

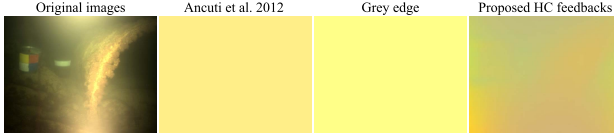


Fig. 2. The light source color map estimated by Ancuti *et al.* [14], Grey edge [50] and our HC feedbacks based method for an underwater image with the obvious nonuniform color bias.

fact that fish eyes are more sensitive to longer wavelength lights [31], [40], [62], [63] and the red component of an underwater image is generally much weaker than its blue and green components, such HC feedbacks in the red channel are calculated globally using the bright parts of the scene so as to avoid the red artifact after CC processing. The HC feedbacks in the three channels are calculated as

$$\begin{aligned} HCF_R(x, y) &= \text{mean}_{f_R > \theta} \{f_R(x, y)\} \text{mean}_{N \times N} \\ HCF_G(x, y) &= \{f_G(x, y)\} \text{mean}_{N \times N} \\ HCF_B(x, y) &= \{f_B(x, y)\} \text{mean}_{N \times N} \end{aligned} \quad (3)$$

where θ is a parameter controlling the selection of the bright parts in the red channel. We set $HCF_R(x, y) = \max(\{f_R\}_{N \times N})$ to control the selection when there is no pixel value higher than θ in the local window $\{f_R\}_{N \times N}$ centered at (x, y) . Fig. 2 shows the significant difference between the estimated light source color map returned by HC feedbacks (i.e., $HCF_\lambda(x, y), \lambda \in \{R, G, B\}$) and two methods usually used for CC processing of an underwater image [14], [50]. Note that our proposed HC feedbacks estimate a spatially varying light source color map, which is quite useful for nonuniform CC since the color attenuation within an underwater image is usually not spectrally uniform [10]. In contrast, the conventional methods always return an uniform light source color map.

With the HC feedbacks, the cone signals become

$$CS_\lambda(x, y) = \frac{f_\lambda(x, y)}{HCF_\lambda(x, y)}, \quad \lambda \in \{R, G, B\} \quad (4)$$

Then, the interplexiform cells release dopamine to inhibit the activity of horizontal cells in dark environment to improve the contrast of image components with the intermediate brightness [64], [65]. Therefore, we further use the *sigmoid* function to suppress the dim part of cone signals after being modulated by HC feedbacks and the final cone signals are

$$CO_\lambda(x, y) = \frac{1}{1 + e^{-10(CS_\lambda(x, y) - 0.5)}}, \quad \lambda \in \{R, G, B\} \quad (5)$$

We can easily get the output of rod cells $CO_{rod}(x, y)$ via Eqs (3)~(5) with the input $L(x, y)$ except that the rod pathway has only one channel (i.e., $\lambda \in L$). Finally, the modulated signals (i.e., $CO_\lambda(x, y)$ and $CO_{rod}(x, y)$) are sent to the layer of bipolar cells with the spatial center-surround RF for locally enhancing the contrasts and edges.

C. Bipolar Cells

The visual signal processing in retina is divided into the ON and OFF pathways from the layer of bipolar cells. Moreover,

the bipolar cells on the rod pathways can excite or inhibit the bipolar cells on the cone pathways via the amacrine cells. Hence, the RF center of the bipolar cells on the cone pathways also receives inputs from the amacrine cells (as indicated by the black and gray arrows from the amacrine cells to bipolar cells in Fig. 1).

We define a two-dimensional Gaussian function as:

$$g_\sigma(x, y) = \frac{1}{2\pi\sigma^2} \exp(-(x^2 + y^2)/(2\sigma^2)) \quad (6)$$

The response of bipolar cells could be calculated by convolving the cone signals with a Difference of Gaussian (DOG) function as:

$$\begin{aligned} Bp(x, y) &= \max[0, (f_{bc} \otimes g_{\sigma_c})(x, y) - k * (f_{bs} \otimes g_{\sigma_s})(x, y)] \\ Bp'(x, y) &= \max[0, (f'_{bc} \otimes g_{\sigma_c})(x, y) \\ &\quad - k * (f'_{bs} \otimes g_{\sigma_s})(x, y)] \end{aligned} \quad (7)$$

where Bp and Bp' denote respectively the outputs of ON and OFF bipolar cells, \otimes indicates the convolution operation. f_{bc} and f_{bs} denote the inputs to the central and surround RF of ON bipolar cells. f'_{bc} and f'_{bs} are the inputs to the central and surround RF of OFF bipolar cells (see Eqs. (10)~(12) for computation). For the rod pathway of bipolar cells, f_{bcL} and f_{bsL} are respectively the signals of rod cells and the signals of rod cells after modulation by the rod horizontal cells:

$$\begin{aligned} f_{bcL} &= CO_{rod}(x, y) \\ f_{bsL} &= \{CO_{rod}(x, y)\} \text{mean}_{N \times N} \end{aligned} \quad (8)$$

Similarly, we can compute the output of rod bipolar cells as:

$$Bp_{rod} = \max[0, (f_{bcL} \otimes g_{\sigma_c})(x, y) - k * (f_{bsL} \otimes g_{\sigma_s})(x, y)] \quad (9)$$

For the cone pathway of bipolar cells, there are two types of inputs. One input is directly from the cones and another one is from the rod bipolar cells after being modulated by amacrine cells. We use the *gamma* correction to simulate the nonlinear modulation of amacrine cells, hence the input to the RF center of cone bipolar cells f_{bc} is given by

$$f_{bc}(x, y) = CO_\lambda(x, y) * Bp_{rod}^\gamma \quad (10)$$

We experimentally set the γ value to 0.5 in this work. f_{bs} is the cone signal locally processed by the horizontal cells, which is treated as the input to the RF surround of cone bipolar cells.

$$f_{bs}(x, y) = \{CO_\lambda(x, y)\} \text{mean}_{N \times N} \quad (11)$$

Finally, the signals along the OFF pathway f'_{bc} and f'_{bs} can be simply obtained by

$$\begin{aligned} f'_{bc} &= 1 - f_{bc} \\ f'_{bs} &= 1 - f_{bs} \end{aligned} \quad (12)$$

In Eqs (7) and (9), the parameters σ_c , σ_s and k need to be determined. σ_c and σ_s are respectively the central and surrounding scales of the DOG, which helps to reduce the image blurriness. σ_s is commonly restricted to the three times of σ_c based on the physiological findings [66]. With extensive experiments, we found that for most of the underwater images,

when σ_c is set between 0.2 to 0.5, the processed images by DOG are clear and insensitive to this parameter, hence we always set $\sigma_c = 0.3$ in this work. k is a weight that controls the inhibition of the RF surround to the RF center.

D. Ganglion Cells

The amounts and types of ganglion cells for processing the red and green components are far more than that for the blue component in the fish visual system [53], [54], [67]. The fine processing of the red and green components at the ganglion level may be an adaption to the bluish underwater environments. To make the final enhanced images more suitable to the sense of human visual system, we choose the single opponent cells with the red-green and blue-yellow color opponent mechanisms to improve the color contrast of images [68]. The RF center and surround of ON and OFF ganglion cells receive the signals from the bipolar cells (i.e., Bp and Bp'), which constitutes the RF of ganglion cells with the red center/green surround, green center/red surround, blue center/yellow surround, and yellow center/blue surround (Fig. 1). The signals of yellow channel are equal to the average of signals of red and green channels from the bipolar cells [69], which are computed as:

$$\begin{aligned} Bp_Y &= (Bp_R + Bp_B)/2 \\ Bp'_Y &= (Bp'_R + Bp'_B)/2 \end{aligned} \quad (13)$$

Finally, the responses of ganglion cells are calculated using a new DOG operation with the color opponency (DOGCO), which are written as

$$\begin{aligned} Gg(x, y) &= \max[0, (f_{gc} \otimes g_{\sigma_c} \\ &\quad + m * (f_{gc} \otimes g_{\sigma_c} - f_{gs} \otimes g_{\sigma_s}))(x, y)] \\ Gg'(x, y) &= \max[0, (f'_{gc} \otimes g_{\sigma_c} \\ &\quad + m * (f'_{gc} \otimes g_{\sigma_c} - f'_{gs} \otimes g_{\sigma_s}))(x, y)] \end{aligned} \quad (14)$$

where Gg and Gg' denote respectively the outputs of ON and OFF ganglion cells, f_{gc} , f_{gs} , f'_{gc} and f'_{gs} represents the signals from the bipolar cells (i.e., Bp and Bp'). Taking the ON-type ganglion cells with the red center/green surround as an example (Fig. 1), its central RF takes the red component of Bp as the input f_{gc} , while its surrounding RF takes the green component of Bp as the input f_{gs} . Similarly, for the OFF-type ganglion cells with the red center/green surround mechanisms, its central RF takes the red component of Bp' as the input f'_{gc} , while its surrounding RF takes the green component of Bp' as the input f'_{gs} . In Eqs (14), σ_c and σ_s are the scales of the central and surrounding RFs of ganglion cells and we set them with the same values as that of bipolar cells. Similarly, m denotes the weight that controls the influence of surrounding RF to the central RF.

The DOGCO operation seems similar to the unsharp masking used in [9]. However, there are three clear differences. 1) The DOGCO operation is calculated in the color opponent space, but the unsharp masking in [9] is computed in the luminance space. 2) The parameter m in DOGCO operation is automatically determined according to the global contrast of the image, but the operation in [9] uses the histogram

stretching technique to avoid the parameter setting. 3) The purpose of DOGCO operation is for color correction and color enhancement, but the purpose of [9] is for sharpening the image that is quite similar to the step of DOG processing in our algorithm. The color-opponent mechanisms used in DOGCO operation provide an adaptive way for adjusting the color appearance of underwater images during enhancement.

E. Automatic Setting of the Parameters k and m According to Adaptive Neural Mechanisms

In Eqs (7) and (14), the interactions between the RF center and surround of bipolar cells and ganglion cells are modeled by a DOG function. However, the efficiency of DOG in transferring the edges and color contrast depends on the appropriate weights of the RF surround (i.e., k and m), which are difficult to tune automatically. Fortunately, a solution has already been found in the mammal visual system in the form of dynamic, contrast-based, center-surround cortical interactions [33], [59], which have not been presented in the HVS inspired formulations [61], [70], [71]. For example, the influence of the surrounding RF on the central RF typically varies depending on the local contrast of both the center and surround, with greater inhibition for higher contrast stimuli [33]. Although the ultimate purpose of these non-linear interactions is not fully known, we speculate that they might play a role in color and contrast enhancement and accordingly, we propose an adaptive model that overcomes the need for ad-hoc or dataset-dependent parameters (and in this sense, it is fully automatic).

Specifically, when the blurriness of an underwater image is relatively high, which corresponds to the low contrast stimuli, a larger k calls more signals of surrounding RF to improve the local contrast [72]. We have found that the parameter k is positively correlated to the dense of haze within the underwater images. Since the dense of haze may act as an indicator for coding the contrast of an underwater image (e.g., higher dense of haze corresponds to lower contrast of image), we directly estimate the dense of haze in the image utilizing DCP [26], which is used as a measure to automatically set the parameter k .

The values of k are roughly proportional to the average dense of haze. Based on the DCP model, $t(x, y)$ in Eq. (1) can be written as:

$$t(x, y) = 1 - \min_{x, y \in \Omega} \left(\min_{\lambda} \frac{I_{\lambda}(x, y)}{A_{\lambda}^{1/4}(x, y)} \right), \quad \lambda \in \{R, G, B\} \quad (15)$$

where Ω is a square patch centered at (x, y) . We estimate the background light $A_{\lambda}(x, y)$ as the estimated nonuniform light source color map:

$$A_{\lambda}(x, y) = HCF_{\lambda}(x, y), \quad \lambda \in \{R, G, B\} \quad (16)$$

Note that the background light $A_{\lambda}(x, y)$ is heterogeneous compared to Eq. (1). Therefore, as opposed to the common assumption in DCP based dehazing [30], the estimated transmission $t(x, y)$ is spatially color-dependent. Since correct depth estimation requires both the background light and the

transmission of an underwater image to be correctly estimated [9], we will quantitatively show that our proposed nonuniform light source color map would help provide better depth estimation than that of the homogeneous background light (see Fig. 13).

Finally, the value of k can be simply calculated using the estimated haze in the image as:

$$k = \text{mean} \left(\min_{x,y \in \Omega} \left(\min_{\lambda} \frac{I_{\lambda}(x,y)}{A_{\lambda}(x,y)} \right) \right) \quad (17)$$

We use the similar adaptive mechanisms to control the setting of parameter m . We found that the values of m are roughly negatively correlated to the saturation of the output image from the bipolar cells. Note that the saturation of image could be treated as a simple measurement of the color contrast of image. The saturation of an image can be calculated as [73]

$$S(x,y) = 1 - \frac{3 \min(Bp_R, Bp_G, Bp_B)}{Bp_R + Bp_G + Bp_B} \quad (18)$$

We take the average of the second term in Eq. (18) over the whole image as the value of m :

$$m = \text{mean} \left(\frac{3 \min(Bp_R, Bp_G, Bp_B)}{Bp_R + Bp_G + Bp_B} \right) \quad (19)$$

The values of m are inversely proportional to the saturation of the output from the bipolar cells. The lower saturation intuitively indicates the higher value of m , thus the greater contributions from the surrounding RF to the central RF, which can help enhance the color contrast of underwater images.

F. Fusion of ON and OFF Channels

We simply use a weighted wavelet method to fuse the signals from the ON-type and OFF-type ganglion cells. The purpose is to combine the advantages of both channels. Moreover, the potential artifacts due to the oversaturated regions of each channel can be minimized during wavelet fusion.

$$\begin{aligned} Output(x,y) = & \text{wavelet}\{w_{ON}(x,y) * Gg(x,y) \\ & + w_{OFF}(x,y) * Gg'(x,y)\}_2 \end{aligned} \quad (20)$$

where w_{ON} and w_{OFF} are the weights controlling respectively the contributions of the signals from the OFF and ON channels. To emphasize the weight of bright parts of images and weaken the weight of dark parts of images, a sigmoid function is introduced

$$F(Gg(x,y)) = \frac{1}{1 + e^{-10(Gg(x,y)-0.5)}} \quad (21)$$

The normalized weight of the ON pathway is

$$w_{ON}(x,y) = \frac{F(Gg(x,y))}{Gg(x,y) + F(Gg(x,y))} \quad (22)$$

and the weight of the OFF pathway is

$$w_{OFF}(x,y) = 1 - w_{ON}(x,y) \quad (23)$$

Note that our fusion of the luminance information processed by the ON and OFF pathways using Eq. (20) is different from other fusion based methods [9], [14], which use various weights to highlight specific regions (e.g., Laplacian contrast weight, saliency weight, saturation weight).

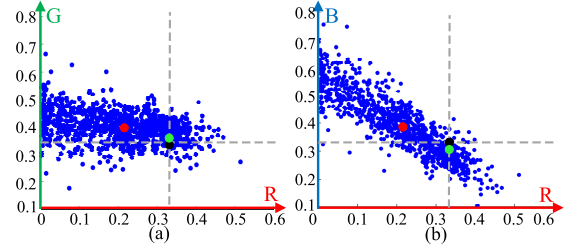


Fig. 3. The color distributions of the underwater images of ImageNet. (a) R vs. G space, (b) R vs. B space. In each panel, each blue dot denotes the average of the estimated light source colors of an image, the red dot denotes the center of all blue dots, the black dot denotes the center of R vs. G and R vs. B space, the green dot denotes the center of the estimated light source colors of all images with $\theta = 0.29$. The location of green dot is very close to the black dot in both R vs. G and R vs. B spaces.

IV. EXPERIMENTS AND COMPARISONS

This section will first show the function of each layer, the influence of parameter settings on the performance in detail, and a comprehensive validation of our proposed nonuniform CC introduced in Section III. We will then compare our method with the existing underwater image restoration/enhancement techniques based on the qualitative and quantitative evaluations on various datasets.

A. Function of Each Layer

1) Horizontal Cells and Nonuniform Color Correction: The processing by the horizontal cells involved in the operations of Eqs (3) and (4) acts as a nonuniform CC approach, but with a parameter θ dependent global compensation for the red channel. We first determined the suitable value of θ using the average statistics of the estimated nonuniform light source colors. We selected the underwater subset (n09376526) of ImageNet as the validation dataset that contains 1069 color images. The images in this subset were captured in various underwater scenes at different depths, which roughly meets the requirement of scene diversity under the nonuniform color bias.

We first set $\theta = 0.0$ for Eq. (3) and the blue dots in Fig. 3 show the average of the estimated nonuniform light source colors of each image in the underwater subset in the R vs. G and R vs. B plots. The centers of these blue dots are denoted by the red dots. We can observe that the red dots locate far away from the centers of R vs. G and R vs. B spaces (i.e., the point with $R = G = 1/3$ or $R = B = 1/3$, as indicated by the black dots in Fig. 3 (a) and (b)). This implies that the red channel is overall weaker than the green and blue channels for most of the underwater images. Thus, we need to adjust the value of θ to compensate the red channel so that the average reflectance of the images is achromatic (i.e., the red dots should coincide with the black dots). Our hypothesis for this step is that normalizing the color distributions by moving the distributions of chromaticities will make their averages roughly converge to the achromatic assumption [77] and will not be sensitive to the color distributions of images, since this subset has already contained many colorful scenes captured by various camera settings.

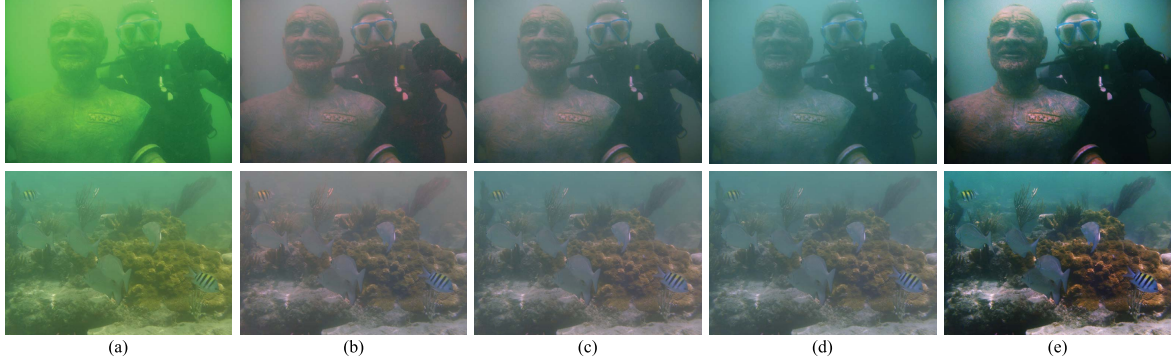


Fig. 4. CC with various values of θ . (a) Original images, (b) $\theta = 0.15$, (c) $\theta = 0.3$, (d) $\theta = 0.45$, and (e) images with the global contrast improvement.

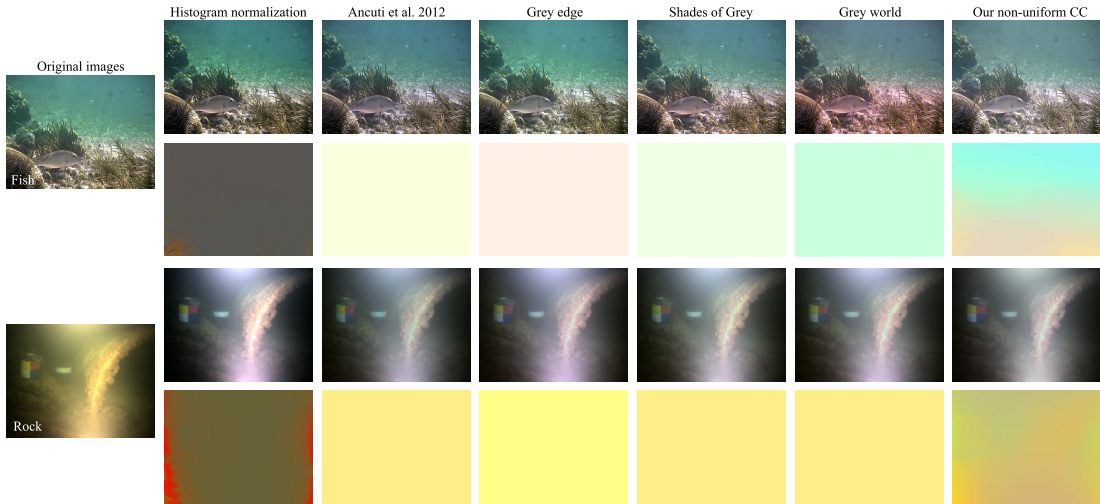


Fig. 5. The results of various approaches on the underwater images with nonuniform color bias. Taking the first underwater image as an example, the first column shows the original image, the second to seventh columns list the corrected images and the corresponding estimated light source colors by different approaches.

By exhaustive searching of θ with a step of 0.01, we found that with $\theta = 0.29$, the centers of the average of the estimated nonuniform light source colors (as indicated by the green dots in Fig. 3) are closest to the black dots. Therefore, we always set $\theta = 0.29$ for the following experiments. To intuitively show the influence of θ on color correction, Fig. 4 gives the results of two underwater images with $\theta = 0.15, 0.3$ and 0.45 . We observe that both images get better color recovery with $\theta = 0.3$ (e.g., Fig. 4 (c)). In contrast, with $\theta = 0.15$, the corrected images present a little reddish appearance (Fig. 4 (b)), while with $\theta = 0.45$, the images appear a little bluish (e.g. Fig. 4 (d)). Fig. 4 (e) shows the results after the global contrast improvement by applying Eq. (5) on Fig. 4 (c).

Another merit of the feedbacks from color-sensitive horizontal cells to cones is to introduce a nonuniform CC processing. Fig. 5 shows the comparisons of CC and the corresponding estimated light source colors for different images with the nonuniform color bias by various approaches. The approaches based on uniform color bias assumption [14], [50], [77], [78] always return an estimated single light source color, which could not effectively remove the nonuniform color bias. For example, the color bias in the images given

by Ancuti et al. 2012 [14] and Grey edge [50] still exists. However, our proposed nonuniform CC approach returns the estimated multiple light source colors, which could well handle the nonuniform color bias in the underwater images. Section IV will present more results of CC for underwater images with nonuniform color bias using quantitative measurements.

2) Bipolar Cells and Ganglion Cells: With an adaptive DOG processing, bipolar cells further improve the local contrast of images and thus help remove the haze. Fig. 6 shows an underwater image enhanced respectively by the ON and OFF pathways of bipolar cells and ganglion cells, where the nonuniform haze is significantly removed. We found that the ON and OFF channels play complementary roles in enhancing the local contrast of images. For example, the DOG processing with ON channel usually leads to oversaturated regions with brighter highlights and darker shadows (e.g, the ROIs in Fig. 6). However, the DOG processing with OFF channel can well preserve the details of bright and dark regions and thus help balance the over-enhanced results by ON channel after fusion (e.g, Fig. 7). Thus, the final output is better than the outputs before fusion qualitatively and quantitatively (i.e., UCIQE = 0.6103 vs. UCIQE = 0.6059 or 0.5736). Though

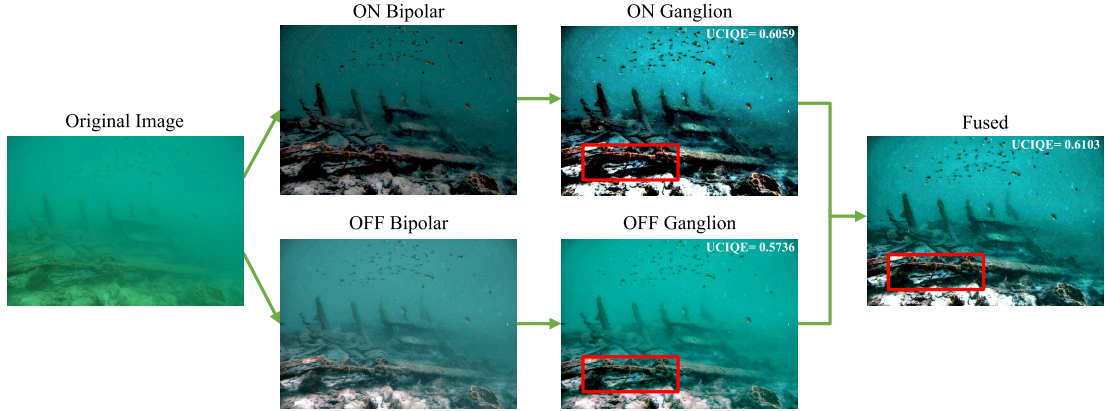


Fig. 6. Illustration of the roles of ON and OFF pathways. The regions of interest (ROIs) are marked with red boxes. The final output is visually better than the outputs before fusion qualitatively and quantitatively. The larger UCIQE score indicates the better quality [80].

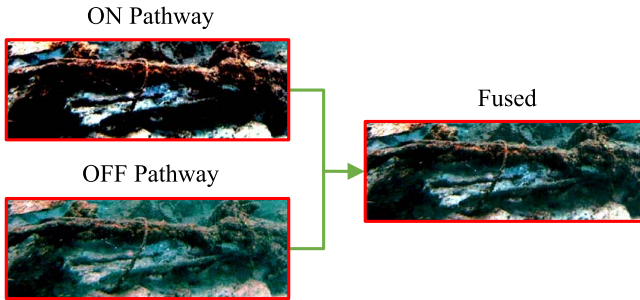


Fig. 7. Zoomed-in view of the ROIs in the images of Fig. 6.

the processing by bipolar cell seems to reduce the color contrast, the following color-opponent processing by ganglion cells can improve the color contrast.

In section III E, we adopt the global statistics of image (e.g., the dense of haze and the color saturation) to automatically control the setting of parameter k and m for guiding the color enhancement and dehazing. To illustrate how the parameters influence the results, we take the ON pathway as an example. We tested various values of k and m in Eqs. (7) and (14), and the results are listed in Fig. 8, in which the results of bipolar layer are shown in the top row and the results of ganglion layer are shown in the bottom row. We can see that with the increasing of the parameter k , the haze in the image is gradually reduced, until some details in the dark parts of image are also suppressed (Note that the fusion with OFF pathway could balance this issue as indicated in Fig. 6 and Fig. 7). The similar trends hold true for the results of color enhancement with ganglion cells shown in the bottom row. With the increase of parameter m , the color saturation of image becomes higher, and thus help enhance the color contrast of image. In this case, our models use the global statistics to automatically calculate the values k as 0.66 and m as 0.71, which provide the performances that are quite close to the images in the fourth column of Fig. 8.

B. Underwater Dehazing and Color Correction Evaluations

We adopted five metrics to quantitatively evaluate the proposed method. The first two are the recently developed under-

water color image quality evaluation metrics: *UCIQE* [80] and *UIQM* [79]. The third metric is the reproduction angular error (*RAE*) that is used to evaluate the performance of color restoration [10], [82]. The fourth metric is the Pearson correlation coefficient (ρ) that measures the correlation between the true depth and the negative logarithm of the estimated transmission map [15]. The ρ has a value between -1 and $+1$, where $+1$ is a perfect correlation, indicating a good transmission estimation, while lower values indicate that the 3D structures of the scenes are not estimated correctly. A negative value implies a wrong estimation of the background light or that the used prior is not valid for that scene [10]. We finally applied an indirect evaluation to demonstrate the usefulness of our approach on assisting to solve the challenging task of local feature point matching [9].

We first evaluated our proposed approach on a new underwater dataset that contains color charts and the 3D structures of the scenes with stereo imaging as the ground truth [10], [15]. We present the results on the RAW images for fair comparison, where we adopted the standard camera pipeline as recommended by Berman *et al.* [15] to convert the RAW data into the format that our method could handle. We used the code provided by the authors of [15] for the calculation of *RAE* and ρ . The results of other methods on this dataset are also cited from Berman *et al.* [15]. As can be observed in Fig. 10, due to the underlying assumption of uniform color bias, the underwater image processing approaches of [27], [29], [76] are not able to consistently correct the colors in the images, and visually, even increase the color bias. In contrast, the underwater processing approaches exploiting the local color properties of images (e.g., the GW assumption with a red channel compensation on highly attenuated local regions in [9], the multiple spectral profiles of different water types in [15], and estimating a nonuniform light source color map proposed by our method) obtain more consistent color appearance and thus the high robustness in preserving the color consistency for different underwater scenes. Our method is rather effective in restoring the colors across different distances, as demonstrated by the color charts on the fourth row of Fig. 10. Table II shows the median and mean *RAE* on the Berman *et al.* dataset [15] for each method. By comparing the input images and the



Fig. 8. The influence of parameter setting on the appearance of processed images. The top row lists the results of bipolar cells with $k = 0.0, 0.2, 0.4, 0.6, 0.8$, the bottom row lists the results of ganglion cells with $m = 0.0, 0.2, 0.4, 0.6, 0.8$.

TABLE I
THE MEASURE OF UIQM, CM, SM, AND CONM [79] ON MULTIPLE IMAGES FOR EACH METHOD IN FIG. 11. LARGER IS BETTER

	He 2011				Drews 2013				Galdran 2015				Ancuti 2016				Berman 2017				Ancuti 2018				Our method			
	CM	SM	ConM	UIQM	CM	SM	ConM	UIQM	CM	SM	ConM	UIQM	CM	SM	ConM	UIQM	CM	SM	ConM	UIQM	CM	SM	ConM	UIQM	CM	SM	ConM	UIQM
Shipwreck	4.304	3.544	0.879	1.106	5.396	5.567	1.299	1.652	6.051	3.819	1.244	1.474	5.787	4.643	1.249	1.539	6.025	4.313	1.157	1.432	5.177	5.575	1.256	1.611	7.061	6.105	1.133	1.553
Coral reef 1	5.829	4.342	1.150	1.426	8.002	4.857	1.333	1.648	5.622	2.876	1.244	1.399	5.742	6.471	1.234	1.663	7.400	4.964	1.259	1.584	6.123	9.019	1.113	1.748	7.334	11.79	0.943	1.811
Diver 1	2.844	1.895	0.821	0.917	3.761	3.204	0.751	0.958	7.532	1.820	0.785	0.912	14.95	3.307	1.095	1.363	9.213	2.022	0.972	1.111	10.46	4.380	1.347	1.643	8.261	3.554	1.459	1.667
Coral reef 2	4.315	2.477	0.896	1.040	3.965	2.231	0.939	1.059	7.401	3.143	1.057	1.261	6.474	3.909	1.194	1.438	9.806	3.336	1.117	1.348	7.987	5.377	1.188	1.555	8.089	7.190	1.253	1.752
Damselfish	15.06	7.800	0.835	1.466	11.64	8.183	1.168	1.775	11.95	5.970	0.985	1.442	12.27	8.741	0.967	1.637	14.88	8.317	1.036	1.687	8.430	14.15	0.805	1.871	10.76	16.91	0.879	2.165
Coral Reef 3	7.083	5.286	1.217	1.568	8.056	6.004	1.309	1.713	6.490	5.415	1.281	1.632	6.150	6.151	1.172	1.585	10.10	6.462	1.193	1.657	6.554	8.053	1.044	1.614	12.91	12.28	0.745	1.705
Diver 2	3.146	4.206	0.835	1.107	3.643	6.723	1.072	1.518	5.777	3.361	0.750	0.984	10.33	4.564	0.969	1.309	6.170	5.580	0.887	1.281	4.897	6.987	0.968	1.453	13.79	7.121	0.985	1.542
Average	6.083	4.221	0.947	1.232	6.351	5.252	1.124	1.474	7.260	3.772	1.049	1.300	8.814	5.398	1.125	1.504	9.084	4.999	1.088	1.442	7.089	7.648	1.103	1.642	9.743	9.278	1.056	1.742

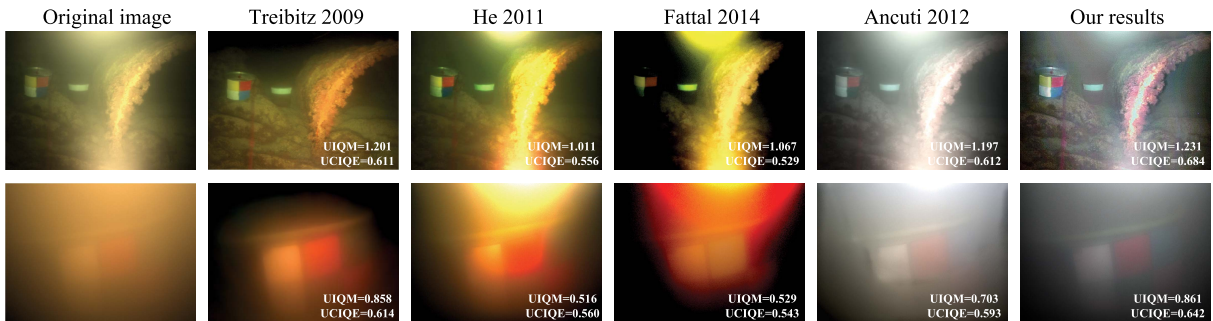


Fig. 9. Underwater dehazing of extreme scenes characterized by the nonuniform illumination condition. Our method performs better than the earlier approaches of Treibitz and Schechner [25], He *et al.* [26], Fattal [74] and Ancuti *et al.* [14].

results by global contrast stretching (i.e., Orig. vs Cont.), we see that a global operation cannot compensate for the distance-dependent color degradation. While the *RAE* of the contrast stretching is often lower than the original input for the closest chart (#1), and this difference often diminishes for farther charts, demonstrating that a nonuniform color correction is required. Our proposed method shows the lowest *RAE* and thus obtains the significantly better CC performance than previous algorithms [9], [27], [29], [76]. Compared to the recent SOTAs, our proposed method also obtains better performance (e.g., 5.44° of our method vs 5.76° of [75] and

7.03° of [15]). Fig. 12 presents the results of our method under various settings of parameter k and m by an exhaustive searching for two examples from Berman *et al.* dataset [15]. Our method can even further obtain better performance of CC if we fine tune each parameter. However, the automatically setting of k and m according to the adaptive neural mechanisms has already allowed to obtain comparable results (e.g., the red star) that are close to those adopting the optimal parameters by an exhaustive search, which further proves the generalizability of our automatic method for real-world application.

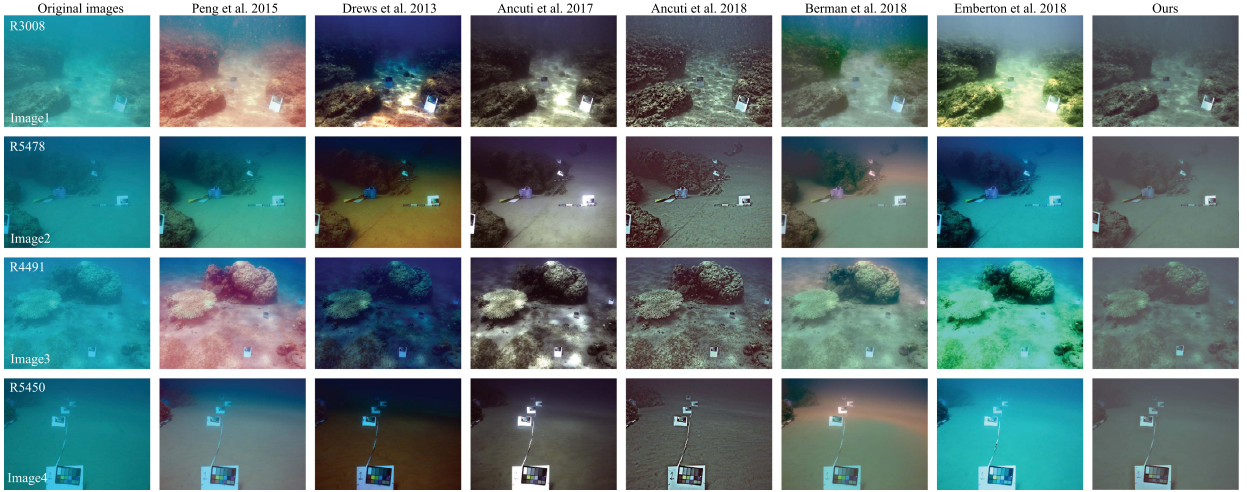


Fig. 10. Comparison of the CC results by different approaches on the challenging underwater scenes. From left to right: the original underwater images, the results by Peng et al. 2015 [29], Drews et al. 2013 [27], Ancuti et al. 2017 [75], Ancuti et al. 2018 [9], Berman et al. 2018 [15], Emberton et al. 2018 [76], and our results. The quantitative measures associated to these images are provided in Table II.

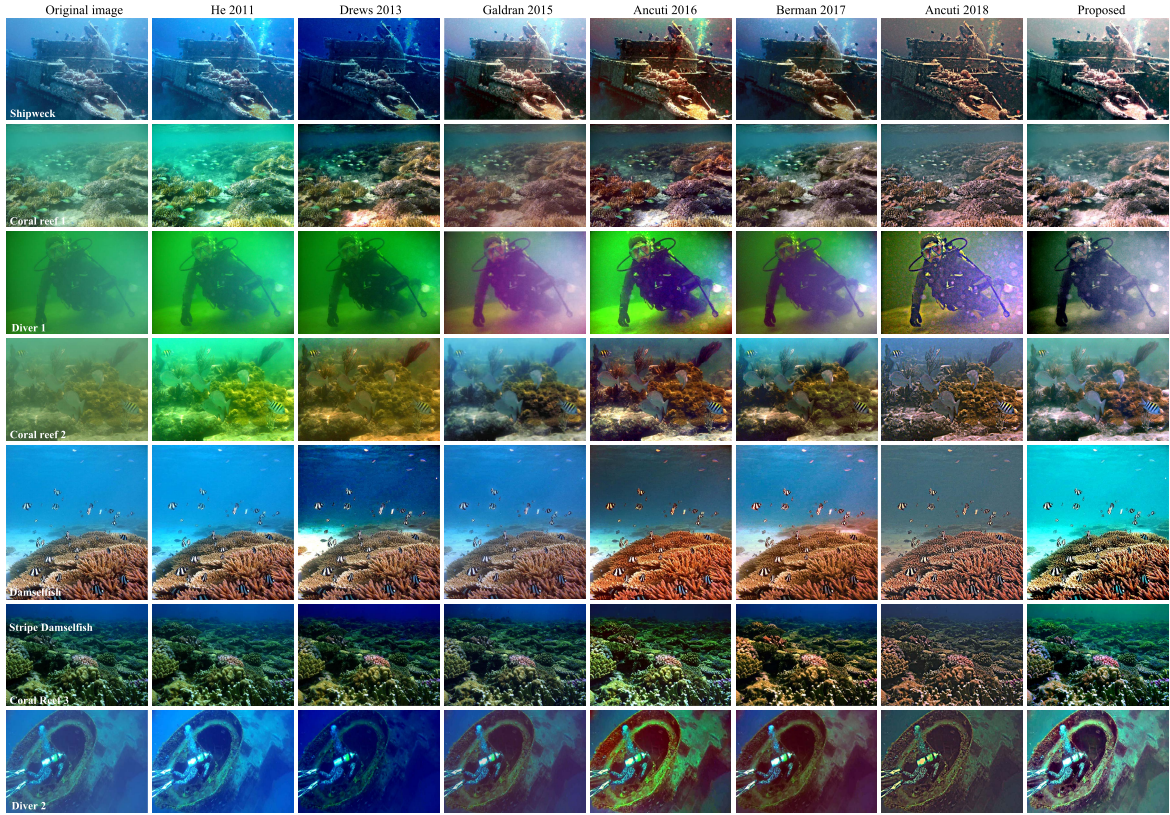


Fig. 11. The results on seven underwater images with various hazes and color bias obtained by the proposed method and the existing outdoor (He *et al.* [26]) and the state-of-the-art underwater dehazing algorithms (Ancuti *et al.* [9], Berman *et al.* [10], Galdran *et al.* [21], Drews *et al.* [27], Ancuti *et al.* [81]). The quantitative evaluation associated to these images is provided in Table I and III.

Fig. 11 further presents the results obtained on seven underwater images [28] by several recent underwater dehazing approaches. Table I and III provides the corresponding quantitative evaluation using the metrics of UIQE [79] and UCIQE [80] specifically designed to evaluate the performance of underwater image enhancement approaches. As can be observed, the outdoor dehazing approach of He *et al.* [26]

performs poorly for the underwater scenes in terms of both color correction and contrast enhancement. The recent underwater dehazing approaches of Galdran *et al.* [21], Drews *et al.* [27], and Ancuti *et al.* [81] show higher robustness than the outdoor method in recovering the visibility of the considered scenes. However, the images processed by these approaches still suffer from the obvious color bias

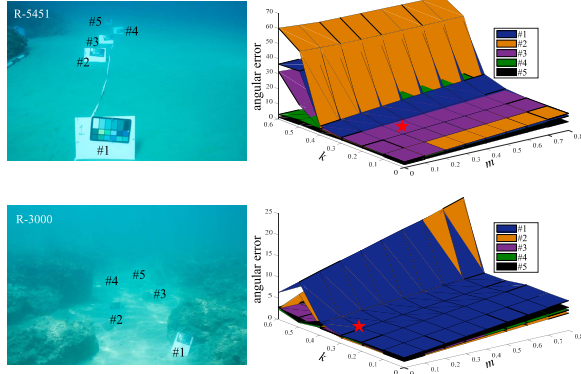


Fig. 12. The average angular error (in terms of RAE) of gray-scale patches measured for different values of k and m . The five color charts are numbered and annotated on the images. The panels on the right column show the RAE for each chart (averaged over the gray-scale patches in the chart). The red stars indicate the locations of the values of k and m automatically determined by our adaptive neural mechanisms.

TABLE II

THE RAE IN RGB SPACE BETWEEN THE GRAY-SCALE PATCHES AND A PURE GRAY COLOR FOR ALL CHARTS IN EACH IMAGE OF BERMAN ET AL. DATASET [15] FOR MULTIPLE METHODS, INCLUDING THE RESULTS ON THE ORIGINAL IMAGES AND THE RESULTS BY GLOBAL CONTRAST STRETCHING (LABELED CONT.). LOWER IS BETTER

Method	Orig.	Cont.	[27]	[29]	[81]	[75]	[9]	[76]	[15]	Ours
R3008#1	29.18	23.73	26.74	3.19	14.89	2.25	5.00	5.14	7.05	4.23
R3008#2	30.48	25.06	43.74	3.98	31.75	2.35	3.63	8.25	6.32	3.49
R3008#3	33.24	32.18	38.20	1.80	8.62	2.27	4.39	5.88	6.71	4.33
R3008#4	34.03	35.23	40.44	2.18	5.30	2.71	3.96	5.80	9.88	3.08
R3008#5	34.08	35.05	40.05	2.62	6.01	4.21	4.91	5.76	8.27	3.46
R3204#1	27.43	19.27	12.81	1.73	23.14	2.79	13.00	6.64	7.58	4.23
R3204#2	34.10	34.32	32.03	7.95	13.07	3.04	4.24	5.08	7.91	3.49
R3204#3	34.11	34.76	35.92	17.36	6.05	4.91	6.14	7.20	9.82	4.33
R3204#4	34.21	34.71	35.66	24.66	5.76	4.76	3.21	7.29	9.12	3.09
R3204#5	34.21	34.84	37.30	28.01	4.17	5.83	4.88	7.62	13.94	3.46
R4376#1	35.17	34.80	37.00	30.29	31.19	6.58	17.05	39.10	25.28	13.06
R4376#2	35.21	34.64	40.27	29.65	33.69	6.85	19.87	37.73	23.80	10.41
R4376#3	35.13	34.70	40.86	31.26	18.61	5.55	16.62	37.04	23.10	7.43
R4376#4	35.96	39.01	39.33	28.61	5.22	11.25	8.47	38.07	14.04	7.15
R4485#1	34.37	34.76	40.39	22.08	15.69	1.74	13.89	36.46	6.36	5.36
R4485#2	34.34	35.30	46.21	33.87	15.38	4.18	9.02	37.91	3.48	5.19
R4485#3	34.54	36.32	42.41	34.71	12.43	3.12	5.91	35.91	1.72	5.34
R4491#1	34.37	35.19	41.76	7.75	21.85	6.30	13.45	33.42	10.14	5.75
R4491#2	34.24	34.68	45.78	6.64	10.98	5.70	10.59	34.26	7.51	7.84
R4491#3	34.29	36.14	44.35	33.92	12.02	9.11	7.54	34.11	4.39	4.89
R5450#1	34.31	34.56	28.25	17.55	18.18	6.73	7.81	27.69	12.93	10.39
R5450#2	34.29	33.86	35.53	28.09	11.44	5.97	13.37	24.74	11.58	5.47
R5450#3	34.45	34.06	36.56	32.92	9.89	7.33	8.90	30.89	2.23	7.68
R5450#4	34.21	33.99	36.66	34.31	9.37	7.98	6.42	32.85	2.38	8.42
R5450#5	34.50	33.65	40.29	34.96	2.87	9.54	4.72	34.48	3.59	2.86
R5469#1	34.28	34.09	20.11	15.85	20.50	4.92	10.17	30.29	7.01	7.69
R5469#2	34.36	34.39	20.67	19.52	9.45	6.26	13.82	34.82	5.20	5.42
R5469#3	34.38	33.98	27.36	23.26	10.95	7.38	7.47	34.38	1.57	8.62
R5469#4	34.42	34.15	29.80	24.99	5.93	7.05	3.09	34.75	2.63	6.79
R5478#1	34.34	34.07	23.51	33.74	25.20	4.80	12.11	31.35	4.20	7.32
R5478#2	34.42	33.95	27.30	34.25	15.67	6.28	5.53	35.28	3.63	7.35
R5478#3	34.50	34.23	32.78	34.43	12.01	9.22	5.27	35.49	2.83	6.49
Mean	33.91	33.55	35.00	21.44	13.98	5.59	8.58	25.49	8.32	6.06
Median	34.32	34.47	36.83	24.82	12.01	5.76	7.51	33.13	7.03	5.44

(e.g., the pictures of Diver 1 and Coral reef 3 in Fig. 11). Our approach outperforms them in color correction, and has similar or in general higher values of the UIQM, CM, SM,

TABLE III

THE MEASURE OF UCIQE [80] ON MULTIPLE UNDERWATER IMAGES FOR EACH METHOD IN FIG. 11. LARGER IS BETTER

Image/Method	Original	He 2011	Drews 2013	Galdran 2015	Ancuti 2016	Berman 2017	Ancuti 2018	Our method
Shipwreck	0.5035	0.5206	0.5482	0.6451	0.6547	0.6263	0.6208	0.6310
Coral reef 1	0.4977	0.5463	0.5795	0.5285	0.6582	0.6218	0.6342	0.6523
Diver 1	0.4125	0.4486	0.4920	0.5236	0.6140	0.5624	0.5925	0.6347
Coral reef 2	0.4263	0.4753	0.5427	0.6035	0.6677	0.6532	0.6361	0.6755
Damselfish	0.6899	0.6948	0.7140	0.6521	0.7307	0.7276	0.6784	0.7352
Coral Reef 3	0.6126	0.6121	0.6002	0.5915	0.6407	0.6854	0.6482	0.6915
Diver 2	0.4908	0.5479	0.5843	0.5569	0.6423	0.6152	0.5904	0.6433
Average	0.5190	0.5494	0.5801	0.5859	0.6583	0.6417	0.6287	0.6662

TABLE IV

EACH ROW SHOWS THE PEARSON CORRELATION COEFFICIENT ρ BETWEEN THE ESTIMATED TRANSMISSION MAPS AND THE GROUND TRUTH DISTANCE FOR A METHOD. SINCE THE DISTANCE IS CALCULATED IN METERS, WE CALCULATE THE CORRELATION BETWEEN THE DISTANCE AND $-\log(t)$ [15]

Image	R3008	R4376	R5478	R4491	R5450	R4485	R5469	R3204	R3158
Drews <i>et al.</i>	-0.28	-0.71	-0.40	-0.45	-0.46	-0.59	-0.43	-0.30	-0.26
Peng <i>et al.</i>	0.72	0.43	0.16	0.06	0.15	0.44	0.13	0.68	0.63
Ancuti <i>et al.</i>	0.01	0.12	0.13	0.06	0.39	0.06	0.04	0.11	0.20
Emberton <i>et al.</i>	-0.04	-0.87	0.11	-0.54	-0.04	-0.74	-0.05	-0.12	0.06
Berman <i>et al.</i>	0.93	0.75	0.66	0.80	0.87	0.73	0.90	0.89	0.81
DCP (uniform)	-0.02	-0.62	-0.41	-0.27	-0.45	-0.25	-0.32	-0.07	0.09
DCP (ours)	0.79	0.74	0.51	0.66	0.47	0.72	0.36	0.60	0.81

ConM, and UCIQE metrics. Compared to the recent multiscale approach proposed in [9] and the method used the prior of water types [10], our proposed method produces images with the higher sharpness and better color correction performance. Our method quantitatively obtains the highest colorfulness measure (CM) and sharpness measure (SM) and thus achieves the best performance in terms of UIQM among all of the approaches. Similarly, our proposed method also significantly outperforms other methods on average by achieving the highest UCIQE score.

We have further processed a set of underwater images that contain the standard Macbeth Color Checker taken by seven different professional cameras [9]. Fig. 14 shows the results of our approach on the underwater images taken with different cameras. It is clear that our approach effectively removes the color variance in the same scenes introduced mainly by the changing of cameras and thus obtains quite consistent color appearance, which further proves the robustness of our method to different camera settings [9].

Fig. 15 presents more results on a recent underwater image dataset proposed by Li *et al.* [17]. This dataset currently includes 890 real-world underwater images collected from the Internet, which possesses diverse color bias and contrast degradation. Compared to five SOTAs including two deep learning-based approaches [16], [30], [83]–[85], our proposed method could effectively remove various color bias within these scenes and thus preserve quite consistent color appearance as already shown in Fig. 11, Fig. 10 and Fig. 14. This further proves the robustness of our proposed method on processing the

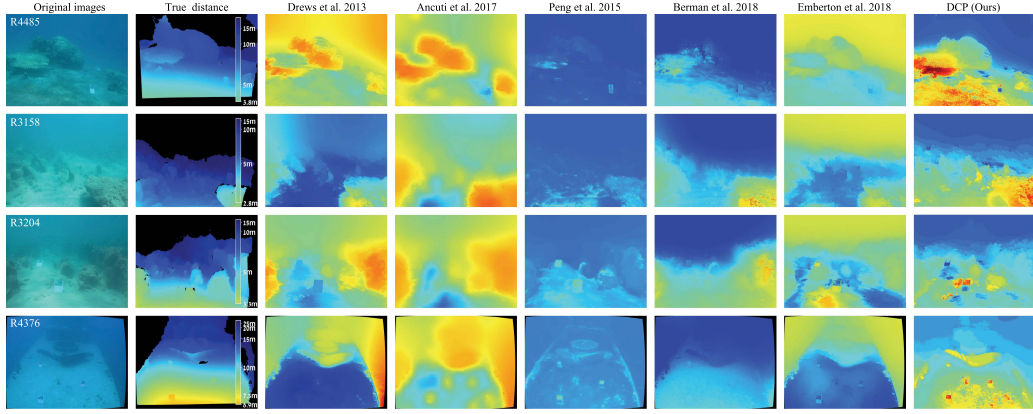


Fig. 13. True distances and estimated transmission maps of each method for some images shown in Table IV.

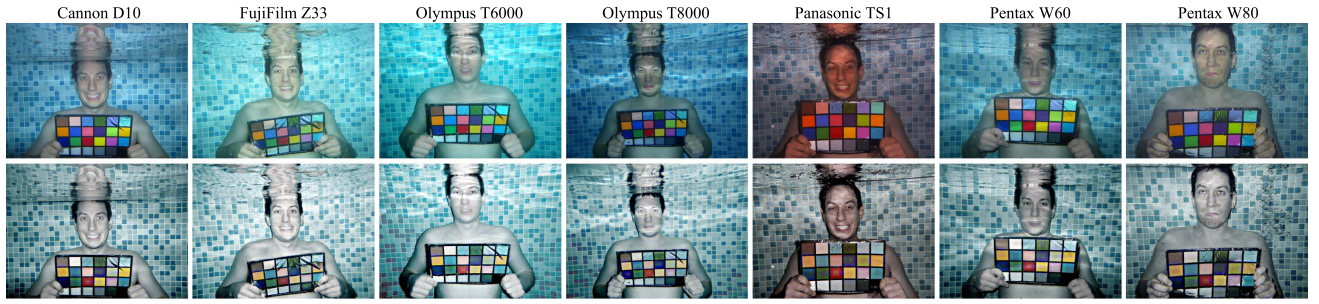


Fig. 14. The results of our approach (the second row) on the underwater images taken with different cameras (the first row). The images are provided by the authors of [9], which were captured approximately one meter away from the subjects using seven different cameras, namely, Canon D10, FujiFilm Z33, Olympus Tough 6000, Olympus Tough 8000, Pentax W60, Pentax W80, Panasonic TS1.

underwater images with various color and contrast degradation issues. Fig. 9 further considers the extreme cases observed in turbid sea water with the nonuniform artificial illumination condition [9], [25], where the images appear quite low contrast and non-uniformly yellowish due to a strong attenuation of the blue channel. Our proposed approach performs better than previous approaches in terms of contrast improvement and color correction.

C. Applications

Table IV shows that our nonuniform light source map strategy yields significant improvement in estimating transmission based on the well-known DCP [26]. As can be seen in Fig. 13, the methods estimating the transmission maps with the uniform light source assumption yield poor estimates. In contrast, the underwater processing approaches [15] employing the space-dependent color properties of images outperform other algorithms in terms of transmission accuracy. The performance of our method using the nonuniform color properties is preceded only by the method proposed by Berman *et al.* [15]. However, their method relies on the specific prior of the water types.

Finally, we employed the SIFT [86] operator to extract the keypoints, and compared the keypoint computation and matching processes for the original and dehazed images. We used the original implementation of SIFT applied exactly in the same way for both cases. The promising improvements

in Fig. 16 demonstrate that by enhancing the global contrast and the local features of the underwater images, the number of the matched pairs of keypoints can be significantly increased.

D. About the Robustness

We all know that the robustness of an underwater image enhancement method is significant because the underwater images have various quality degradation issues, and the robustness seems a most serious problem of current methods [7], [18], [27], [28]. However, the introduced mechanisms and strategies make our method roughly insensitive to the parameter settings. For example, in order to automatically set the parameters k and m involved in the DOG models for the bipolar cells and ganglion cells, we proposed an adaptive way imitating the contrast-based center-surround cortical interaction mechanisms [33], [59] to overcome the need for ad-hoc or dataset-dependent parameters. Specifically, the parameters k and m are inversely proportional to the contrast of images, which can adaptively enhance the color contrast for the underwater images with low contrast or low color saturation, as indicated by Fig. 8, Fig. 10, Fig. 11, Fig. 12, Fig. 14 and Fig. 15. For example, from the results presented in Fig. 10, Fig. 11, Fig. 14 and Fig. 15, with the automatic setting of k and m we can observe that our proposed method can effectively remove various color bias contained in these scenes and thus preserve quite consistent

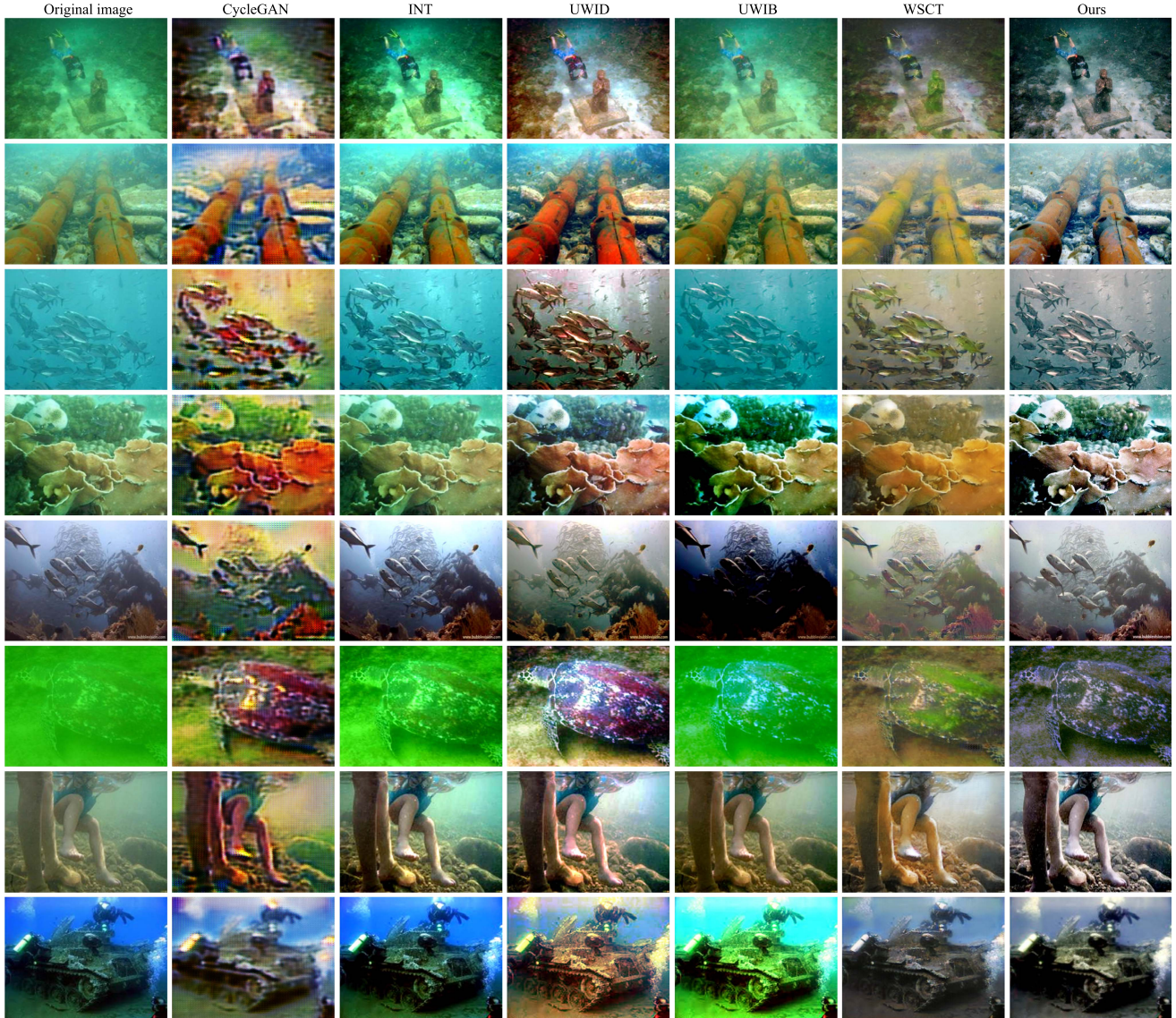


Fig. 15. More results on a large underwater dataset [17] with various hazes and color bias obtained by the proposed method and the state-of-the-art underwater image enhancing algorithms including INT [83], UWID [84], UWIB [30], and the deep learning-based CycleGAN [85] and WSCT [16].

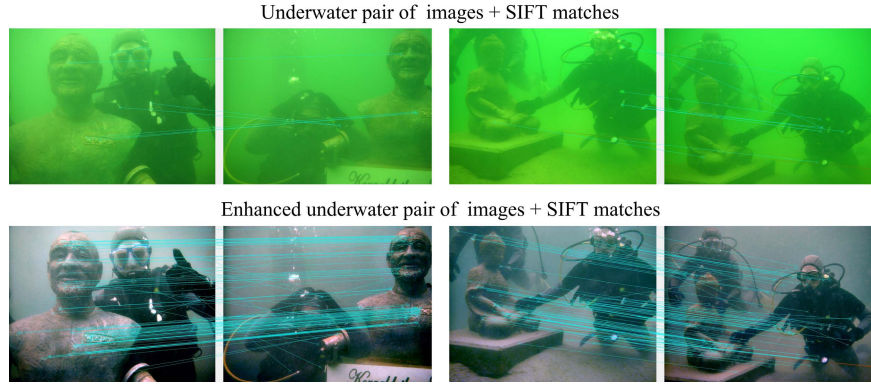


Fig. 16. Applying the standard SIFT on our enhanced versions (bottom) improves considerably the point matching process compared to the results on the original images (top).

color appearance. In addition, our approach also performs quite robust to the images taken by different camera settings (i.e., Fig. 14).

V. CONCLUSION

In this work, we proposed a new underwater image enhancement model by carefully considering the features of the

underwater environments and the adaptive mechanisms of the teleost fish retina. Extensive experiments on different underwater datasets show that our method can simultaneously eliminate the haze and the nonuniform color bias. Compared to the SOTAs, our technique produces very competitive performance in terms of both qualitative and quantitative evaluations. Moreover, for the first time, we demonstrate the values of modeling the visual mechanisms of underwater creatures for the challenging underwater image processing tasks [1], [24].

We attribute the promising results of this work to the following differences between this work and other existing methods for underwater image processing. i) We introduced a nonuniform color correction algorithm, which could well handle the nonuniform color cast in underwater images compared to the existing methods that were usually built on the uniform color cast condition. ii) We imitated the adaptive retinal mechanisms to control the model parameters of each low-level filter according to the global contrast of a given image, which overcomes the need for ad-hoc or dataset-dependent parameters (and in this sense, it is fully automatic). iii) We exploited the color-opponent mechanisms to flexibly adjust the color appearance of underwater images during image enhancement. iv) Our algorithm introduced the complementary fusion of luminance information given by the ON and OFF pathways of the retina, which is different from those fusion based methods [9], [14] using various weights (e.g., Laplacian contrast weight, saliency weight, saturation weight).

ACKNOWLEDGMENT

The authors would like to thank Dr. Miao Yang, Dr. Yan-Tsung Peng for sharing the codes of their work, Dr. Cosmin Ancuti for sharing the images in Fig. 9 and Fig. 14, and Dr. Dana Berman *et al.* for sharing their datasets and codes for evaluation.

REFERENCES

- [1] R. Schettini and S. Corchs, "Underwater image processing: State of the art of restoration and image enhancement methods," *EURASIP J. Adv. Signal Process.*, vol. 2010, Dec. 2010, Art. no. 746052.
- [2] E. Trucco and A. T. Olmos-Antillon, "Self-tuning underwater image restoration," *IEEE J. Ocean. Eng.*, vol. 31, no. 2, pp. 511–519, Apr. 2006.
- [3] H. Lu, Y. Li, and S. Serikawa, "Underwater image enhancement using guided trigonometric bilateral filter and fast automatic color correction," in *Proc. IEEE Int. Conf. Image Process.*, Sep. 2013, pp. 3412–3416.
- [4] A. Arnold-Bos, J. P. Malkasse, and G. Kervern, "Towards a model-free denoising of underwater optical images," in *Proc. IEEE Eur. Oceans Conf.*, Brest, France, vol. 1, Jun. 2005, pp. 527–532.
- [5] S. Bazeille, I. Quidu, L. Jaulin, and J.-P. Malkasse, "Automatic underwater image pre-processing," in *Proc. CMM*, 2006, p. 20.
- [6] F. Petit, A.-S. Capelle-Laize, and P. Carre , "Underwater image enhancement by attenuation inversion with quaternions," in *Proc. IEEE Int. Conf. Acoust., Speech Signal Process.*, Apr. 2009, pp. 1177–1180.
- [7] M. Bryson, M. Johnson-Roberson, O. Pizarro, and S. B. Williams, "True color correction of autonomous underwater vehicle imagery," *J. Field Robot.*, vol. 33, no. 6, pp. 853–874, 2016.
- [8] M. Bryson, M. Johnson-Roberson, O. Pizarro, and S. Williams, "Colour consistent structure-from-motion models using underwater imagery," in *Proc. Int. conf. Robot. Sci. Syst.*, 2012, pp. 33–40.
- [9] C. O. Ancuti, C. Ancuti, C. De Vleeschouwer, and P. Bekaert, "Color balance and fusion for underwater image enhancement," *IEEE Trans. Image Process.*, vol. 27, no. 1, pp. 379–393, Jan. 2018.
- [10] D. Berman, T. Treibitz, and S. Avidan, "Diving into haze-lines: Color restoration of underwater images," in *Proc. Brit. Mach. Vis. Conf. (BMVC)*, vol. 1, no. 2, 2017, pp. 1–12.
- [11] X. Fu, P. Zhuang, Y. Huang, Y. Liao, X.-P. Zhang, and X. Ding, "A retinex-based enhancing approach for single underwater image," in *Proc. IEEE Int. Conf. Image Process. (ICIP)*, Oct. 2014, pp. 4572–4576.
- [12] J. Y. Chiang and Y.-C. Chen, "Underwater image enhancement by wavelength compensation and dehazing," *IEEE Trans. Image Process.*, vol. 21, no. 4, pp. 1756–1769, Apr. 2012.
- [13] B. Henke, M. Vahl, and Z. Zhou, "Removing color cast of underwater images through non-constant color constancy hypothesis," in *Proc. 8th Int. Symp. Image Signal Process. Anal. (ISPA)*, Sep. 2013, pp. 20–24.
- [14] C. Ancuti, C. O. Ancuti, T. Haber, and P. Bekaert, "Enhancing underwater images and videos by fusion," in *Proc. IEEE Conf. Comput. Vis. Pattern Recognit.*, Jun. 2012, pp. 81–88.
- [15] D. Berman, D. Levy, S. Avidan, and T. Treibitz, "Underwater single image color restoration using haze-lines and a new quantitative dataset," Nov. 2018, *arXiv:1811.01343*. [Online]. Available: <https://arxiv.org/abs/1811.01343>
- [16] C. Li, J. Guo, and C. Guo, "Emerging from water: Underwater image color correction based on weakly supervised color transfer," *IEEE Signal Process. Lett.*, vol. 25, no. 3, pp. 323–327, Mar. 2018.
- [17] C. Li *et al.*, "An underwater image enhancement benchmark dataset and beyond," Jan. 2019, *arXiv:1901.05495*. [Online]. Available: <https://arxiv.org/abs/1901.05495>
- [18] J. Li, K. A. Skinner, R. M. Eustice, and M. Johnson-Roberson, "WaterGAN: Unsupervised generative network to enable real-time color correction of monocular underwater images," *IEEE Robot. Autom. Lett.*, vol. 3, no. 1, pp. 387–394, Jan. 2018.
- [19] N. Carlevaris-Bianco, A. Mohan, and R. M. Eustice, "Initial results in underwater single image dehazing," in *Proc. OCEANS MTS/IEEE SEATTLE*, Sep. 2010, pp. 1–8.
- [20] H. Lu, Y. Li, L. Zhang, and S. Serikawa, "Contrast enhancement for images in turbid water," *J. Opt. Soc. Amer. A, Opt. Image Sci.*, vol. 32, no. 5, pp. 886–893, 2015.
- [21] A. Galdran, D. Pardo, A. Picón, and A. Alvarez-Gila, "Automatic red-channel underwater image restoration," *J. Vis. Commun. Image Represent.*, vol. 26, pp. 132–145, Jan. 2015.
- [22] S. G. Narasimhan and S. K. Nayar, "Vision and the atmosphere," *Int. J. Comput. Vis.*, vol. 48, no. 3, pp. 233–254, 2002.
- [23] S. G. Narasimhan and S. K. Nayar, "Chromatic framework for vision in bad weather," in *Proc. IEEE Conf. Comput. Vis. Pattern Recognit. (CVPR)*, vol. 1, Jun. 2000, pp. 598–605.
- [24] D. M. Kocak, F. R. Dalglish, F. M. Caimi, and Y. Y. Schechner, "A focus on recent developments and trends in underwater imaging," *Mar. Technol. Soc. J.*, vol. 42, no. 1, pp. 52–67, 2008.
- [25] T. Treibitz and Y. Y. Schechner, "Active polarization descattering," *IEEE Trans. Pattern Anal. Mach. Intell.*, vol. 31, no. 3, pp. 385–399, Mar. 2009.
- [26] K. He, J. Sun, and X. Tang, "Single image haze removal using dark channel prior," *IEEE Trans. Pattern Anal. Mach. Intell.*, vol. 33, no. 12, pp. 2341–2353, Dec. 2011.
- [27] P. Drews, E. do Nascimento, F. Moraes, S. Botelho, and M. Campos, "Transmission estimation in underwater single images," in *Proc. IEEE Int. Conf. Comput. Vis. Workshops*, Dec. 2013, pp. 825–830.
- [28] S. Emberton, L. Chittka, and A. Cavallaro, "Hierarchical rankbased veiling light estimation for underwater dehazing," in *Proc. Brit. Mach. Vis. Conf. (BMVC)*, X. Xie, M. W. Jones, and G. K. L. Tam, Eds. Surrey, U.K.: BMVA Press, Sep. 2015, pp. 125.1–125.12. doi: [10.5244/C.29.125](https://doi.org/10.5244/C.29.125).
- [29] Y.-T. Peng, X. Zhao, and P. C. Cosman, "Single underwater image enhancement using depth estimation based on blurriness," in *Proc. IEEE Int. Conf. Image Process. (ICIP)*, Sep. 2015, pp. 4952–4956.
- [30] Y.-T. Peng and P. C. Cosman, "Underwater image restoration based on image blurriness and light absorption," *IEEE Trans. Image Process.*, vol. 26, no. 4, pp. 1579–1594, Apr. 2017.
- [31] R. H. Douglas and M. B. A. Djamgoz, Eds., *The Visual System of Fish*. London, U.K.: Chapman & Hall, 1990.
- [32] N. A. Locket, "Adaptations to the deep-sea environment," in *Handbook of Sensory Physiology*, vol. 7/5, F. Crescitelli, Ed. Berlin, Germany: Springer, 1977, pp. 67–192.
- [33] A. Angelucci and S. Shushruth, "Beyond the classical receptive field: Surround modulation in primary visual cortex," in *The New Visual Neurosciences*, L. M. Chalupa and J. S. Werner, Eds. Cambridge, MA, USA: MIT, 2013.
- [34] R. Douglas and C. Hawryshyn, "Behavioural studies of fish vision: An analysis of visual capabilities," in *The Visual System of Fish*, R. Douglas and M. Djagoz, Eds. Amsterdam, The Netherlands: Springer, 1990, pp. 373–418.

- [35] C. Neumeyer, "On spectral sensitivity in the goldfish: Evidence for neural interactions between different 'cone mechanisms,'" *Vis. Res.*, vol. 24, no. 10, pp. 1223–1231, 1984.
- [36] F. Harosi, "Correlation between cone absorbance and horizontal cell response from 300 to 700 nm in fish," *Invest. Ophthalmol. Vis. Sci.*, vol. 27, p. 192, Feb. 1986.
- [37] C.-C. Chiao, T. W. Cronin, and D. Osorio, "Color signals in natural scenes: Characteristics of reflectance spectra and effects of natural illuminants," *J. Opt. Soc. Amer. A, Opt. Image Sci.*, vol. 17, no. 2, pp. 218–224, 2000.
- [38] C.-C. Chiao, M. Vorobyev, T. W. Cronin, and D. Osorio, "Spectral tuning of dichromats to natural scenes," *Vis. Res.*, vol. 40, no. 23, pp. 3257–3271, 2000.
- [39] S. Johnsen, E. A. Widder, and C. D. Mobley, "Propagation and perception of bioluminescence: Factors affecting counterillumination as a cryptic strategy," *Biol. Bull.*, vol. 207, no. 1, pp. 1–16, 2004.
- [40] J. E. Dowling, "Dopamine: A retinal neuromodulator?," *Trends Neurosci.*, vol. 9, pp. 236–240, Jan. 1986.
- [41] A. Kaneko and M. Yamada, "S-potentials in the dark-adapted retina of the carp," *J. Physiol.*, vol. 227, no. 1, pp. 261–273, 1972.
- [42] J. E. G. Downing, "Functionally identified interneurons in the vertebrate (fish) retina: Electrophysiological ultrastructural and pharmacological studies," Ph.D. dissertation, Dept. Pure Appl. Biol., Univ. London, London, U.K., 1983.
- [43] R. Weiler, "Horizontal cells of the carp retina: Golgi impregnation and procion-yellow injection," *Cell Tissue Res.*, vol. 195, no. 3, pp. 515–526, 1978.
- [44] M. Kamermans and H. Spekreijse, "Spectral behavior of cone-driven horizontal cells in Teleost Retina," *Prog. Retinal Eye Res.*, vol. 14, no. 1, pp. 313–360, 360.
- [45] D. J. Ingle, "The goldfish as a retinex animal," *Science*, vol. 227, no. 4687, pp. 651–655, 1985.
- [46] S. Zeki, "The representation of colours in the cerebral cortex," *Nature*, vol. 284, no. 5755, pp. 412–418, 1980.
- [47] M. Kamermans, D. A. Kraaij, and H. Spekreijse, "The cone/horizontal cell network: A possible site for color constancy," *Vis. Neurosci.*, vol. 15, no. 5, pp. 787–797, 1998.
- [48] M. VanLeeuwen, C. Joselevitch, I. Fahrenfort, and M. Kamermans, "The contribution of the outer retina to color constancy: A general model for color constancy synthesized from primate and fish data," *Vis. Neurosci.*, vol. 24, no. 3, pp. 277–290, 2007.
- [49] S. Sabbah, C. Zhu, M. A. Hornsby, M. Kamermans, and C. W. Hawryshyn, "Feedback from horizontal cells to cones mediates color induction and may facilitate color constancy in rainbow trout," *PLoS ONE*, vol. 8, no. 6, Jun. 2013, Art. no. e66216.
- [50] J. van de Weijer, T. Gevers, and A. Gijsenij, "Edge-based color constancy," *IEEE Trans. Image Process.*, vol. 16, no. 9, pp. 2207–2214, Sep. 2007.
- [51] A. Ishida, W. Stell, and D. Lightfoot, "Rod and cone inputs to bipolar cells in goldfish retina," *J. Comparative Neurol.*, vol. 191, no. 3, pp. 315–335, 1980.
- [52] E. V. Famiglietti, A. Kaneko, and M. Tachibana, "Neuronal architecture of on and off pathways to ganglion cells in carp retina," *Science*, vol. 198, no. 4323, pp. 1267–1269, 1977.
- [53] N. W. Daw, "Colour-coded ganglion cells in the goldfish retina: Extension of their receptive fields by means of new stimuli," *J. Physiol.*, vol. 197, no. 3, pp. 567–592, 1968.
- [54] H. Spekreijse, H. G. Wagner, and M. L. Wolbarsht, "Spectral and spatial coding of ganglion cell responses in goldfish retina," *J. Neurophysiol.*, vol. 35, no. 1, pp. 73–86, 1972.
- [55] D. J. Margolis and P. B. Detwiler, "Different mechanisms generate maintained activity in on and off retinal ganglion cells," *J. Neurosci.*, vol. 27, no. 22, pp. 5994–6005, 2007.
- [56] E. Chichilnisky and R. S. Kalmar, "Functional asymmetries in on and off ganglion cells of primate retina," *J. Neurosci.*, vol. 22, no. 7, pp. 2737–2747, 2002.
- [57] K. A. Zaghloul, K. Boahen, and J. B. Demb, "Different circuits for on and off retinal ganglion cells cause different contrast sensitivities," *J. Neurosci.*, vol. 23, no. 7, pp. 2645–2654, Apr. 2003.
- [58] Z. Nichols, S. Nirenberg, and J. Victor, "Interacting linear and nonlinear characteristics produce population coding asymmetries between on and off cells in the retina," *J. Neurosci.*, vol. 33, no. 37, pp. 14958–14973, 2013.
- [59] S. Shushruth, J. M. Ichida, J. B. Levitt, and A. Angelucci, "Comparison of spatial summation properties of neurons in macaque v1 and v2," *J. Neurophysiol.*, vol. 102, no. 4, pp. 2069–2083, 2009.
- [60] C. Brown, "Fish intelligence, sentience and ethics," *Animal Cognition*, vol. 18, no. 1, pp. 1–17, Jan. 2015.
- [61] X.-S. Zhang, S.-B. Gao, R.-X. Li, X.-Y. Du, C.-Y. Li, and Y.-J. Li, "A retinal mechanism inspired color constancy model," *IEEE Trans. Image Process.*, vol. 25, no. 3, pp. 1219–1232, Mar. 2016.
- [62] J. N. Lythgoe, *The Ecology of Vision*. Oxford, U.K.: Clarendon, 1979.
- [63] J. Lythgoe, "Visual pigments and environmental light," *Vis. Res.*, vol. 24, no. 11, pp. 1539–1550, 1984.
- [64] S. C. Mangel and J. E. Dowling, "The interplexiform–horizontal cell system of the fish retina: Effects of dopamine, light stimulation and time in the dark," *Proc. Roy. Soc. London Ser. B, Biol. Sci.*, vol. 231, no. 1262, pp. 91–121, 1987.
- [65] J. E. Dowling and B. Ehinger, "The interplexiform cell system—I. Synapses of the dopaminergic neurons of the goldfish retina," *Proc. Roy. Soc. London B, Biol. Sci.*, vol. 201, no. 1142, pp. 7–26, 1978.
- [66] R. Shapley and M. J. Hawken, "Color in the cortex: Single-and double-opponent cells," *Vis. Res.*, vol. 51, no. 7, pp. 701–717, Apr. 2011.
- [67] N. Daw, "Neurophysiology of color vision," *Physiol. Rev.*, vol. 53, no. 3, pp. 571–611, 1973.
- [68] K. T. Mullen, "The contrast sensitivity of human colour vision to red-green and blue-yellow chromatic gratings," *J. Physiol.*, vol. 359, no. 1, pp. 381–400, Feb. 1985.
- [69] D. M. Dacey and B. B. Lee, "The 'blue-on' opponent pathway in primate retina originates from a distinct bistratified ganglion cell type," *Nature*, vol. 367, no. 6465, pp. 731–735, 1994.
- [70] X.-S. Zhang, S.-B. Gao, C.-Y. Li, and Y.-J. Li, "A retina inspired model for enhancing visibility of hazy images," *Frontiers Comput. Neurosci.*, vol. 9, p. 151, Dec. 2015.
- [71] S.-B. Gao, K.-F. Yang, C.-Y. Li, and Y.-J. Li, "Color constancy using double opponency," *IEEE Trans. Pattern Anal. Mach. Intell.*, vol. 37, no. 10, pp. 1973–1985, Oct. 2015.
- [72] U. D. Behrens and H. J. Wagner, "Adaptation-dependent changes of bipolar cell terminals in fish retina: Effects on overall morphology and spinule formation in Ma and Mb cells," *Vis. Res.*, vol. 36, no. 24, pp. 3901–3911, 1996.
- [73] R. C. Gonzalez and R. E. Woods, "Digital image processing," in *Digital Restoration of Film and Video Archives*. Reading, MA, USA: Addison-Wesley, 1993, pp. 6–1–6–5.
- [74] R. Fattal, "Single image dehazing," *ACM Trans. Graph.*, vol. 27, no. 3, p. 72, Aug. 2008.
- [75] C. O. Ancuti, C. Ancuti, C. De Vleeschouwer, L. Neumann, and R. Garcia, "Color transfer for underwater dehazing and depth estimation," in *Proc. IEEE Int. Conf. Image Process. (ICIP)*, Sep. 2017, pp. 695–699.
- [76] S. Emberton, L. Chittka, and A. Cavallaro, "Underwater image and video dehazing with pure haze region segmentation," *Comput. Vis. Image Underst.*, vol. 168, pp. 145–156, Mar. 2018.
- [77] G. Buchsbaum, "A spatial processor model for object colour perception," *J. Franklin Inst.*, vol. 310, no. 1, pp. 1–26, Jul. 1980.
- [78] G. D. Finlayson and E. Trezzi, "Shades of gray and colour constancy," in *Proc. 12th Color Imag. Conf., Color Sci., Syst. Appl., Soc. Imag. Sci. Technol.*, 2004, pp. 37–41.
- [79] K. Panetta, C. Gao, and S. Agaian, "Human-visual-system-inspired underwater image quality measures," *IEEE J. Ocean. Eng.*, vol. 41, no. 3, pp. 541–551, Jul. 2016.
- [80] M. Yang and A. Sowmya, "An underwater color image quality evaluation metric," *IEEE Trans. Image Process.*, vol. 24, no. 12, pp. 6062–6071, Dec. 2015.
- [81] C. Ancuti, C. O. Ancuti, C. De Vleeschouwer, R. Garcia, and A. C. Bovik, "Multi-scale underwater descattering," in *Proc. 23rd Int. Conf. Pattern Recognit. (ICPR)*, Dec. 2016, pp. 4202–4207.
- [82] G. D. Finlayson, R. Zakizadeh, and A. Gijsenij, "The reproduction angular error for evaluating the performance of illuminant estimation algorithms," *IEEE Trans. Pattern Anal. Mach. Intell.*, vol. 39, no. 7, pp. 1482–1488, Jul. 2017.
- [83] Y. Gong and I. F. Sbalzarini, "A natural-scene gradient distribution prior and its application in light-microscopy image processing," *IEEE J. Sel. Topics Signal Process.*, vol. 10, no. 1, pp. 99–114, Feb. 2016.
- [84] C.-Y. Li, J.-C. Guo, R.-M. Cong, Y.-W. Pang, and B. Pang, "Underwater image enhancement by dehazing with minimum information loss and histogram distribution prior," *IEEE Trans. Image Process.*, vol. 25, no. 12, pp. 5664–5677, Dec. 2016.

- [85] J.-Y. Zhu, T. Park, P. Isola, and A. A. Efros, "Unpaired image-to-image translation using cycle-consistent adversarial networks," in *Proc. IEEE Int. Conf. Comput. Vis. (ICCV)*, Oct. 2017, pp. 2242–2251.
- [86] D. G. Lowe, "Distinctive image features from scale-invariant keypoints," *Int. J. Comput. Vis.*, vol. 60, no. 2, pp. 91–110, Nov. 2004.



Shao-Bing Gao received the Ph.D. degree in biomedical engineering from the University of Electronic Science and Technology of China in 2017. He is currently a tenure-track Associate Professor with the Neuromorphic Computing Research Center, College of Computer Science, Sichuan University. His research interests include visual mechanism modeling and image processing.



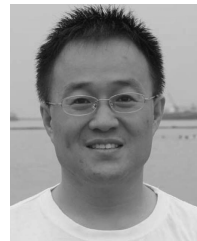
Ming Zhang received the master's degree in biomedical engineering from the University of Electronic Science and Technology of China in 2018. His research interests include visual mechanism modeling and image processing.



Qian Zhao received the B.Sc. degree in biomedical engineering from the University of Electronic Science and Technology of China in 2016, where she is currently pursuing the master's degree in biomedical engineering. Her research interests include image processing.



Xian-Shi Zhang received the Ph.D. degree in biomedical engineering from the University of Electronic Science and Technology of China (UESTC) in 2017. He is currently a Research Assistant Professor with the School of Life Science and Technology, UESTC. His research interests include visual mechanism modeling and image processing.



Yong-Jie Li received the Ph.D. degree in biomedical engineering from the University of Electronic Science and Technology of China (UESTC), China, in 2004. He is currently a Professor with the Key Laboratory for Neuroinformation of Ministry of Education, UESTC. His research interests include visual mechanism modeling and image processing.